

Frascati, Oct. 1st, 1991

Note: **I-4****DAΦNE ACCUMULATOR UPDATE - 2**

S. Guiducci, M.R. Masullo. C. Milardi, M. Preger

**1 - INTRODUCTION**

The general philosophy of injection into DAΦNE, the Frascati Φ-Factory project, is described in [1], together with a preliminary lattice and its chromaticity correction scheme [2]. In this report we summarize the updated accumulator design, including substantial changes in the lattice, a better chromatic correction, tracking studies of injection, an orbit correction scheme, aperture requirements and tolerances on alignment and magnetic field quality. It should be pointed out that the accumulator is designed to accept a positron beam from the Linac with a rather large emittance (10 mm.mrad) and energy spread ( $\pm 1.5\%$ ).

**2 - THE MAGNETIC LATTICE**

The total length of the accumulator has been increased by  $\approx 1$  m, to maintain the ratio of 1/3 to the main ring one. Following the decision of giving up the option of including sextupole windings in the quadrupoles, the extra space has been distributed between the drifts in the dispersive arcs, in order to better accommodate 10 cm long sextupoles near the quadrupoles. For the same reason the length of the free straight sections has been slightly decreased from 3.85 to 3.50 m.

Tracking simulations showed that vanishing dispersion in the injection straight section helps significantly in reducing aperture requirements. To obtain this goal the magnetic periodicity has been halved from 4 to 2, giving up the symmetry axis in the center of the dispersive section. The machine has still a 4-fold mechanical symmetry (if sextupoles are not taken into account), but the currents in the quadrupoles are now divided into 3 independent families instead of 2. This new arrangement, together with a  $\approx 10\%$  increase in the quadrupole length, requires weaker gradients in the quads ( $\approx 4.0 \text{ m}^{-2}$  instead of  $5.3 \text{ m}^{-2}$ ).

Due to the relatively small bending radius (1.1 m), the sharp edge approximation for the field cannot be used. In order to better simulate the bending magnet fringing fields, the actual field profile has been represented by three steps within 10 cm ( $\approx 2$  gap heights) on each side of the magnetic edge corresponding to the rectangular model. The difference between the two magnet models reflects into a  $\approx 10\%$  shift in the vertical betatron tune.

Table I shows a MAD output for the linear lattice, while the optical functions in one fourth of the ring are plotted in Fig. 1. Fig. 2 shows a schematic layout of the ring: the RF cavity has been placed in the injection straight with vanishing dispersion, but the option of having it between K1 and K2 is still open. Table II is an updated list for the accumulator lattice and beam parameters. Table III shows the magnetic structure at the nominal working point.

### 3 - INJECTION AND EXTRACTION

The strategy of injection into DAΦNE is described in [1]: particles are injected at 50 Hz from the Linac into the accumulator, extracted at 1 Hz and injected into the main ring. During each cycle 45 pulses are stored into the accumulator, then there is a 100 ms waiting time to almost completely damp the beam before extraction and injection into the main ring.

As shown in Fig. 2, a symmetric arrangement has been adopted for the kickers, in order to inject both electrons and positrons with the same orbit perturbation. Four fast kickers are fired with the proper delays: K1 and K2 drive the stored beam near the injection septum while K3 and K4 are used downstream to cancel the perturbation on the stored beam and to strongly decrease the oscillation amplitude of the particles coming from the Linac. K5 is used only for extraction, together with K3 and K4. With this configuration it is not necessary to use double polarity power supplies. Moreover, the field value does not change between injection and extraction in one of the two downstream kickers, while in the other one the field is almost doubled. The pulse length of the kickers should not exceed two revolution periods (200 ns). Table IV gives the integrated magnetic fields in the kickers required in the different operation phases (electron/positron/injection/extraction), while Fig. 3 shows the trajectories of the stored beam at injection and extraction.

The injection parameters of the incoming beam have been chosen taking into account mechanical constraints and typical beam parameters for positrons at the nominal energy of the DAΦNE main ring (510 MeV). The injection septum is placed at  $\approx 30$  cm from the edge of the bending magnet (see Fig. 2), and its thickness is 4.2 mm, to allow d.c. operation outside the vacuum chamber. Since the horizontal betatron function is not flat at the septum (see Fig. 1) the beam coming from the Linac will be injected with a small negative angle (towards the inside of the ring) of 6.5 mrad on average.

Tracking studies have been performed to determine the best shape in phase space for the beam coming from the Linac and the required aperture in the accumulator. The simulation takes into account the effect of the chromaticity correction sextupoles as non linear point-like perturbations. The particles start from the injection septum, are tracked through the kickers and followed for 500 turns in the ring. The injection septa act as aperture limits at 20 mm from the ideal orbit on the inner side of the ring. No alignment and field errors are taken into account, and synchrotron oscillations and damping are neglected as well.

**TABLE I**  
**MAD output for the accumulator lattice**

TITLE!  
OTTICA ACCUMULATORE

! PHYSICAL ELEMENTS FOLLOW

DRIFT,L1,L=1.45  
DRIFT,L2,L=0.24943  
DRIFT,L3 L=0.479  
DRIFT,L4 L=0.416  
DRIFT,L5,L=0.15  
DRIFT,L6,L=0.265

QUAD,OF1,L=0.34,K1=3.868414  
QUAD,QD1,L=0.34,K1=-3.965089  
QUAD,OF2,L=0.34,K1=3.559854  
SBEND,B1,L=.034,ANGLE=0.007n,K1=-0.02582  
SBEND,B2,L=.034,ANGLE=0.01545,K1=-0.10329  
SBEND,B3,L=.034,ANGLE=0.02318,K1=-0.23240  
SBEND,BB,L=0.381,ANGLE=0.34634,K1=-0.41316

! LATTICE STRUCTURE FOLLOWS  
LINE,HCELL1=(L1,L2,B1,B2,B3,BB,BB,B3,B2,B1,L3,QF1,L4,QD1)  
LINE,HCELL2=(L4,QF2,L3,B1,B2,B3,BB,BB,B3,B2,B1,L2,L1)  
LINE,HCELL=(HCELL1,HCELL2)  
LINE,PER=(HCELL,-HCELL)  
LINE,MACC=(2\*PER)

| POS. NO.       | ELEMENT NAME | SEQUENCE NO. | DIST [M]     | HORIZONTAL |        |            |            |               |        |        | VERTICAL   |        |           |            |               |        |       |
|----------------|--------------|--------------|--------------|------------|--------|------------|------------|---------------|--------|--------|------------|--------|-----------|------------|---------------|--------|-------|
|                |              |              |              | BETAX [M]  | ALFAX  | MUX [2PI]  | X(CO) [MM] | X'(CO) [MRAD] | DX [M] | DX'    | BETAY [M]  | ALFAY  | MUY [2PI] | Y(CO) [MM] | Y'(CO) [MRAD] | DY [M] | DY'   |
| BEGIN          | MACC         | 1            | 0.000        | 1.332      | 0.000  | 0.000      | 0.000      | 0.000         | 0.000  | 0.000  | 5.264      | 0.000  | 0.000     | 0.000      | 0.000         | 0.000  | 0.000 |
| BEGIN          | HCELL        | 1            | 0.000        | 1.332      | 0.000  | 0.000      | 0.000      | 0.000         | 0.000  | 0.000  | 5.264      | 0.000  | 0.000     | 0.000      | 0.000         | 0.000  | 0.000 |
| BEGIN          | HCELL1       | 1            | 0.000        | 1.332      | 0.000  | 0.000      | 0.000      | 0.000         | 0.000  | 0.000  | 5.264      | 0.000  | 0.000     | 0.000      | 0.000         | 0.000  | 0.000 |
|                | L1           | 1            | 1.450        | 2.910      | -1.089 | 0.132      | 0.000      | 0.000         | 0.000  | 0.000  | 5.664      | -0.275 | 0.043     | 0.000      | 0.000         | 0.000  | 0.000 |
|                | L2           | 1            | 1.699        | 3.500      | -1.276 | 0.144      | 0.000      | 0.000         | 0.000  | 0.000  | 5.813      | -0.323 | 0.050     | 0.000      | 0.000         | 0.000  | 0.000 |
|                | B1           | 1            | 1.733        | 3.588      | -1.298 | 0.146      | 0.000      | 0.000         | 0.000  | 0.008  | 5.835      | -0.324 | 0.051     | 0.000      | 0.000         | 0.000  | 0.000 |
|                | B2           | 1            | 1.767        | 3.676      | -1.311 | 0.147      | 0.000      | 0.000         | 0.001  | 0.023  | 5.856      | -0.310 | 0.052     | 0.000      | 0.000         | 0.000  | 0.000 |
|                | B3           | 1            | 1.801        | 3.765      | -1.306 | 0.149      | 0.000      | 0.000         | 0.002  | 0.046  | 5.876      | -0.270 | 0.052     | 0.000      | 0.000         | 0.000  | 0.000 |
|                | BB           | 1            | 2.182        | 4.602      | -0.846 | 0.163      | 0.000      | 0.000         | 0.085  | 0.388  | 5.754      | 0.583  | 0.063     | 0.000      | 0.000         | 0.000  | 0.000 |
|                | BB           | 2            | 2.563        | 5.004      | -0.187 | 0.176      | 0.000      | 0.000         | 0.294  | 0.706  | 5.022      | 1.300  | 0.074     | 0.000      | 0.000         | 0.000  | 0.000 |
|                | B3           | 2            | 2.597        | 5.016      | -0.155 | 0.177      | 0.000      | 0.000         | 0.319  | 0.726  | 4.933      | 1.320  | 0.075     | 0.000      | 0.000         | 0.000  | 0.000 |
|                | B2           | 2            | 2.631        | 5.026      | -0.144 | 0.178      | 0.000      | 0.000         | 0.344  | 0.741  | 4.843      | 1.318  | 0.076     | 0.000      | 0.000         | 0.000  | 0.000 |
|                | B1           | 2            | 2.665        | 5.036      | -0.147 | 0.179      | 0.000      | 0.000         | 0.369  | 0.748  | 4.754      | 1.303  | 0.077     | 0.000      | 0.000         | 0.000  | 0.000 |
|                | L3           | 1            | 3.144        | 5.223      | -0.244 | 0.194      | 0.000      | 0.000         | 0.727  | 0.748  | 3.636      | 1.031  | 0.096     | 0.000      | 0.000         | 0.000  | 0.000 |
|                | QF1          | 1            | 3.484        | 3.356      | 4.890  | 0.206      | 0.000      | 0.000         | 0.806  | -0.300 | 4.665      | -4.497 | 0.110     | 0.000      | 0.000         | 0.000  | 0.000 |
|                | L4           | 1            | 3.900        | 0.572      | 1.802  | 0.254      | 0.000      | 0.000         | 0.682  | -0.300 | 9.193      | -6.389 | 0.120     | 0.000      | 0.000         | 0.000  | 0.000 |
|                | QD1          | 1            | 4.240        | 0.239      | -0.677 | 0.484      | 0.000      | 0.000         | 0.734  | 0.620  | 9.169      | 6.450  | 0.125     | 0.000      | 0.000         | 0.000  | 0.000 |
| END            | HCELL1       | 1            | 4.240        | 0.239      | -0.677 | 0.484      | 0.000      | 0.000         | 0.734  | 0.620  | 9.169      | 6.450  | 0.125     | 0.000      | 0.000         | 0.000  | 0.000 |
| BEGIN          | HCELL2       | 1            | 4.240        | 0.239      | -0.677 | 0.484      | 0.000      | 0.000         | 0.734  | 0.620  | 9.169      | 6.450  | 0.125     | 0.000      | 0.000         | 0.000  | 0.000 |
|                | L4           | 2            | 4.656        | 1.858      | -3.216 | 0.591      | 0.000      | 0.000         | 0.992  | 0.620  | 4.607      | 4.517  | 0.136     | 0.000      | 0.000         | 0.000  | 0.000 |
|                | QF2          | 1            | 4.996        | 3.441      | -0.783 | 0.611      | 0.000      | 0.000         | 0.991  | -0.623 | 3.406      | -0.513 | 0.150     | 0.000      | 0.000         | 0.000  | 0.000 |
|                | L3           | 2            | 5.475        | 4.299      | -1.007 | 0.631      | 0.000      | 0.000         | 0.693  | -0.623 | 3.983      | -0.691 | 0.171     | 0.000      | 0.000         | 0.000  | 0.000 |
|                | B1           | 3            | 5.509        | 4.368      | -1.019 | 0.632      | 0.000      | 0.000         | 0.672  | -0.616 | 4.030      | -0.700 | 0.172     | 0.000      | 0.000         | 0.000  | 0.000 |
|                | B2           | 3            | 5.543        | 4.437      | -1.020 | 0.633      | 0.000      | 0.000         | 0.651  | -0.603 | 4.078      | -0.698 | 0.174     | 0.000      | 0.000         | 0.000  | 0.000 |
|                | B3           | 3            | 5.577        | 4.506      | -1.000 | 0.635      | 0.000      | 0.000         | 0.631  | -0.585 | 4.124      | -0.678 | 0.175     | 0.000      | 0.000         | 0.000  | 0.000 |
|                | BB           | 3            | 5.958        | 5.036      | -0.363 | 0.647      | 0.000      | 0.000         | 0.457  | -0.323 | 4.429      | -0.104 | 0.189     | 0.000      | 0.000         | 0.000  | 0.000 |
|                | BB           | 4            | 6.339        | 5.038      | 0.359  | 0.659      | 0.000      | 0.000         | 0.387  | -0.042 | 4.277      | 0.494  | 0.203     | 0.000      | 0.000         | 0.000  | 0.000 |
|                | B3           | 4            | 6.373        | 5.012      | 0.391  | 0.660      | 0.000      | 0.000         | 0.386  | -0.021 | 4.243      | 0.518  | 0.204     | 0.000      | 0.000         | 0.000  | 0.000 |
|                | B2           | 4            | 6.407        | 4.985      | 0.400  | 0.661      | 0.000      | 0.000         | 0.386  | -0.007 | 4.207      | 0.522  | 0.205     | 0.000      | 0.000         | 0.000  | 0.000 |
|                | B1           | 4            | 6.441        | 4.958      | 0.397  | 0.662      | 0.000      | 0.000         | 0.385  | 0.000  | 4.172      | 0.516  | 0.207     | 0.000      | 0.000         | 0.000  | 0.000 |
|                | L2           | 2            | 6.691        | 4.775      | 0.338  | 0.671      | 0.000      | 0.000         | 0.385  | 0.000  | 3.934      | 0.440  | 0.217     | 0.000      | 0.000         | 0.000  | 0.000 |
|                | L1           | 2            | 8.141        | 4.284      | 0.000  | 0.723      | 0.000      | 0.000         | 0.385  | 0.000  | 3.296      | 0.000  | 0.282     | 0.000      | 0.000         | 0.000  | 0.000 |
| END            | HCELL2       | 1            | 8.141        | 4.284      | 0.000  | 0.723      | 0.000      | 0.000         | 0.385  | 0.000  | 3.296      | 0.000  | 0.282     | 0.000      | 0.000         | 0.000  | 0.000 |
| END            | HCELL        | 1            | 8.141        | 4.284      | 0.000  | 0.723      | 0.000      | 0.000         | 0.385  | 0.000  | 3.296      | 0.000  | 0.282     | 0.000      | 0.000         | 0.000  | 0.000 |
| END            | MACC         | 1            | 32.563       | 1.332      | 0.000  | 2.890      | 0.000      | 0.000         | 0.000  | 0.000  | 5.264      | 0.000  | 1.130     | 0.000      | 0.000         | 0.000  | 0.000 |
| TOTAL LENGTH = |              |              | 32.563440    |            |        |            |            |               |        |        |            |        |           |            |               |        |       |
|                |              |              |              |            |        | GX         | =          | 2.890013      |        |        | GY         | =      | 1.129986  |            |               |        |       |
|                |              |              |              |            |        | GX'        | =          | -4.388035     |        |        | GY'        | =      | -3.684643 |            |               |        |       |
| ALFA           | =            |              | 0.571390E-01 |            |        | BETAX(MAX) | =          | 5.222732      |        |        | BETAY(MAX) | =      | 9.193260  |            |               |        |       |
| GAMMA(TR)      | =            |              | 4.183443     |            |        | DX(MAX)    | =          | 0.991923      |        |        | DY(MAX)    | =      | 0.000000  |            |               |        |       |

**TABLE II**  
**Parameter List**

---

|   |       |
|---|-------|
| Energy (GeV)  | 0.51  |
| Circumference (m)                                       | 32.56 |
| Straight section length (m)                             | 3.50  |
| Horizontal betatron wavenumber                          | 2.89  |
| Vertical betatron wavenumber                            | 1.13  |
|   |       |
| Dispersion at Septum Straight Section Center (SSSC) (m) | 0.00  |
| Horizontal $\beta$ at SSSC (m)                          | 1.33  |
| Vertical $\beta$ at SSSC (m)                            | 5.26  |
| Dispersion at Kicker Straight Section Center (KSSC) (m) | 0.39  |
| Horizontal $\beta$ at KSSC (m)                          | 4.28  |
| Vertical $\beta$ at KSSC (m)                            | 3.29  |
| Horizontal r.m.s. beam size at SSSC (mm, no coupling)   | 0.63  |
| Vertical r.m.s. beam size at SSSC (mm, full coupling)   | 0.88  |
| Horizontal r.m.s. beam size at KSSC (mm, no coupling)   | 1.14  |
| Vertical r.m.s. beam size at KSSC (mm, full coupling)   | 0.70  |
|   |       |
| Maximum dispersion (m)                                  | 1.04  |
| Maximum horizontal $\beta$ (m)                          | 5.20  |
| Maximum vertical $\beta$ (m)                            | 10.28 |
|   |       |
| Horizontal betatron damping time (msec)                 | 21.42 |
| Vertical betatron damping time (msec)                   | 21.42 |
| Synchrotron damping time (msec)                         | 10.71 |
| Momentum compaction                                     | 0.057 |
| Natural emittance (mm·mrad)                             | 0.294 |
| R.m.s. energy spread (%)                                | 0.042 |
| Horizontal chromaticity (sextupoles off)                | -4.4  |
| Vertical chromaticity (sextupoles off)                  | -3.7  |
|   |       |
| R.F. frequency (MHz)                                    | 73.65 |
| R.F. voltage (KV)                                       | 200   |
| Harmonic number   | 8     |
| Radiated energy per turn (KeV)                          | 5.17  |
| Synchrotron frequency (KHz)                             | 49.12 |
| R.F. energy acceptance (%)                              | 2.3   |
| R.m.s. bunch length (cm) radiation only                 | 2.3   |
| R.m.s. bunch length (cm) $Z/n = 2\Omega$                | 3.8   |
| R.m.s. bunch length (cm) $Z/n = 4\Omega$                | 4.8   |
| Total beam lifetime (min)                               | 52    |

---

**TABLE III**  
Magnetic Structure

---

**Bending magnets**

|                     |       |
|---------------------|-------|
| Number              | 8     |
| Bending angle (deg) | 45    |
| Bending radius (m)  | 1.1   |
| Magnetic length (m) | 0.864 |
| Center field (T)    | 1.55  |
| Field index         | 0.5   |
| Gradient (T/m)      | 0.70  |
| Gap (mm)            | 42    |

---

**Quadrupoles**

|                      |    |
|----------------------|----|
| Number               | 12 |
| Magnetic length (cm) | 34 |
| Bore radius (cm)     | 5  |

| Quadrupole | Strength (m <sup>-2</sup> ) | Gradient (T/m) | Pole field (T) |
|------------|-----------------------------|----------------|----------------|
| Q1         | 3.87                        | 6.58           | 0.329          |
| Q2         | 3.97                        | 6.75           | 0.337          |
| Q3         | 3.56                        | 6.06           | 0.303          |

---

**Sextupoles (for positive chromaticity  $C_x = C_y = +1$ )**

|                      |    |
|----------------------|----|
| Number               | 8  |
| Magnetic length (cm) | 10 |
| Bore radius (cm)     | 5  |

| Sextupole | Strength (m <sup>-3</sup> ) | Gradient (T/m <sup>2</sup> ) | Pole field (T) |
|-----------|-----------------------------|------------------------------|----------------|
| SF        | 63.6                        | 108.1                        | 0.135          |
| SD        | 59.7                        | 101.6                        | 0.127          |

---

With these assumptions a positron beam with an emittance of 10 mm.mrad and  $\pm 1.5\%$  energy spread can be stored into the accumulator with full efficiency. The assumptions on Linac beam parameters are conservative with respect to the values achieved for LIL, the injector of the LEP injection chain ( $\approx 6$  mm.mrad and  $\pm 1.0\%$ ). Figures 4 and 5 show the horizontal and vertical envelopes for 1000 particles entering the ring from the injection septum and performing the first full revolution into the machine, including the angular perturbation given by kickers K3 and K4. Figures 6 and 7 are the envelopes for the other 499 revolutions. Because of the non linear fields in the kickers and sextupoles, it is rather difficult to calculate analytically the optimum shape in horizontal phase space for the beam coming from the Linac. The best configuration has been therefore determined by running tracking simulations. The obtained results shown in Figs. 4÷7 correspond to random extraction of initial coordinates with uniform distributions in the 5 variables X, X', Y, Y',  $\Delta E/E$  in the following ranges:

$$\begin{aligned} -31.8 \leq X \leq -24.2 \text{ (mm)} & & -9.0 \leq X' \leq -4.0 \text{ (mrad)} \\ -7.7 \leq Y \leq 7.7 \text{ (mm)} & & -1.3 \leq Y' \leq 1.3 \text{ (mrad)} \\ & & -1.5\% \leq \Delta E/E \leq +1.5\% \end{aligned}$$

Figure 8 shows the angular deflection given by the kickers as a function of the particle horizontal position at the kicker, calculated from the simple model of four current wires placed at the corners of a 80 mm wide and 30 mm high rectangle centered on the reference orbit. The higher and lower "wings" correspond to the second and first kicker seen by the incoming particles respectively. The width of the wings is due to the energy distribution of the particles. The energy deviation of each particle is also taken into account in the quadrupole and sextupole gradients and the bending magnet radius. For the bending magnet the "three step model" has been adopted while the kicker length ( $\approx 0.5$  m) has been simulated by subdividing each one into three equally spaced point-like angular perturbations.

From the inspection of the envelopes shown in Figures 4÷7 it is possible to set stay-clear requirements on the vacuum chamber design, because other items, such as beam lifetime, can be neglected with respect to injection. Including a reasonable safety margin to allow for closed orbit and field errors (not taken into account at the present stage),  $\pm 15$  mm will be sufficient in the vertical plane, while  $\pm 40$  mm are necessary in the horizontal. A slightly larger aperture in the horizontal plane should be provided, to leave space for the first full oscillation of the beam (see Fig. 4), in the magnetic elements of the arcs downstream the injection septa for both electrons and positrons. This enlargement is necessary to preserve high injection efficiency and to reduce beam losses on the vacuum chamber walls and therefore shielding requirements.

As shown in Table IV, the magnetic field in the kickers has always the same sign in all injection and extraction configurations. For each type of particles only one kicker must change its field intensity between injection and extraction (in less than 20 msec). With the proposed configuration particles are extracted at the septum at a distance of 28.4 mm from the reference orbit with a small angle of 0.4 mrad towards the inside of the ring.

**TABLE IV**  
**Kicker fields**

| Integrated field (Gauss m) | K1   | K2   | K3   | K4   | K5   |
|----------------------------|------|------|------|------|------|
| Positron injection         | 83.7 | 45.7 | 45.7 | 83.7 |      |
| Positron extraction        |      |      | 83.7 | 83.7 | 83.7 |
| Electron injection         | 45.7 | 83.7 | 83.7 | 45.7 |      |
| Electron extraction        |      |      | 83.7 | 83.7 | 83.7 |

#### 4 - CLOSED ORBIT CORRECTION

As already discussed in the preceding section, a rather large aperture is required to accept the large emittance and energy spread of the positron beam from the Linac with good efficiency. Closed orbit distortions decrease the effective acceptance of the ring, and therefore a closed orbit correction scheme is necessary; by keeping the maximum orbit deviations within 2 mm in the horizontal plane and within 1 mm in the vertical the acceptance is reduced by less than 5% and we assumed these figures as a goal for the correction system. The possibility of mechanical displacements of the quadrupoles in both transverse directions is foreseen to further improve orbit correction.

The sensitivity of the lattice to alignment and field errors has been studied using the computer code MAD. The code generates a random distribution of errors with a given standard deviation and then calculates the orbit deviation through the lattice. We have assumed "typical" errors from the experience of operating accelerators, namely 0.2 mm for quadrupole and bending magnet misalignments ( $\Delta x$ ,  $\Delta y$ ), 0.25 mrad for tilts around the transverse axes ( $\Delta\theta$ ,  $\Delta\phi$ ) and magnetic field errors ( $\Delta B/B$ ) of  $5 \times 10^{-4}$ . For each case, 10 machines have been simulated and the average results are shown.

Table V gives the average and maximum orbit deviations obtained by simulating the quoted error distributions separately, i.e. only misalignments in the quads, misalignments in the bending magnets, tilts in the quads etc. These simulations have been performed with all sextupoles switched off. It can be seen that the "first day" closed orbit is expected to be rather sensitive to quadrupole misalignment and field errors in bending magnets.

Monitor and corrector positions are mainly dictated by available space in the structure. The proposed layout is shown in Fig. 8/A: it foresees 10 beam position monitors and 8 correctors, each acting in both planes. The correction has been simulated with MAD, and the results (with sextupoles off) are given in Table VI. The residual orbit is rather satisfactory, with maximum distortions of  $\approx 1.5$  mm in the horizontal plane, and  $\approx 0.5$  mm in the vertical one. The same exercise has been performed with the chromaticity correcting sextupoles on, and Table VII shows the results. Fig. 9 shows the measured beam positions at the monitors before and after correction in the horizontal plane for one of the simulated machines, and Fig. 10 is the corresponding one for the vertical. Fig. 11 is a display of the orbit in the whole machine before correction as calculated by MAD. Monitor alignment errors have also been considered, with standard deviation in the transverse direction of 0.2 mm. The orbit parameters averaged over 10 machines are shown in Table VIII.

**TABLE V**  
**Closed orbit distortion due to single types of errors**

| Type of error                                    |                | in quadrupoles | in bending magnets |
|--|----------------|----------------|--------------------|
| $\Delta x, \Delta y = 0.2 \text{ mm}$            | $X_{rms}$ (mm) | $2.8 \pm 2.0$  | $0.6 \pm 0.3$      |
|  | $X_{max}$ (mm) | $4.6 \pm 3.1$  | $1.0 \pm 0.5$      |
|  | $Y_{rms}$ (mm) | $5.2 \pm 1.6$  | $0.7 \pm 0.3$      |
|  | $Y_{max}$ (mm) | $9.4 \pm 2.9$  | $1.5 \pm 0.6$      |
| $\Delta \Theta, \Delta \Phi = 0.25 \text{ mrad}$ | $X_{rms}$ (mm) | $0.4 \pm 0.1$  | $0.3 \pm 0.2$      |
|  | $X_{max}$ (mm) | $0.7 \pm 0.2$  | $0.5 \pm 0.3$      |
|  | $Y_{rms}$ (mm) | $0.7 \pm 0.2$  | $0.6 \pm 0.2$      |
|  | $Y_{max}$ (mm) | $1.1 \pm 0.3$  | $1.2 \pm 0.4$      |
| $\Delta B/B = 5 \times 10^{-4}$                  | $X_{rms}$ (mm) |                | $3.7 \pm 1.4$      |
|  | $X_{max}$ (mm) |                | $7.0 \pm 2.5$      |

**TABLE VI**  
**Closed orbit parameters before and after correction**  
**10 monitors, 8 correctors (sextupoles off)**  
 $\Delta x = \Delta y = 0.2 \text{ mm}, \Delta \Theta = \Delta \Phi = 0.25 \text{ mrad}, \Delta B/B = 5 \times 10^{-4}$

|                         | ideal machine | before correction | after correction |
|-------------------------|---------------|-------------------|------------------|
| $X_{rms}$ (mm)          | 0             | $5.5 \pm 3.6$     | $0.5 \pm 0.2$    |
| $X_{max}$ (mm)          | 0             | $9.2 \pm 5.1$     | $1.4 \pm 0.3$    |
| $Y_{rms}$ (mm)          | 0             | $3.0 \pm 1.4$     | $0.2 \pm 0.1$    |
| $Y_{max}$ (mm)          | 0             | $5.6 \pm 2.3$     | $0.5 \pm 0.2$    |
| $\eta x_{rms}$ (cm)     | 66.4          | $75.2 \pm 12.7$   | $65.5 \pm 0.2$   |
| $\eta x_{max}$ (cm)     | 100.3         | $132.1 \pm 24.6$  | $101.1 \pm 0.2$  |
| $\eta y_{rms}$ (cm)     | 0             | $9.0 \pm 5.3$     | $0.4 \pm 0.2$    |
| $\eta y_{max}$ (cm)     | 0             | $14.8 \pm 8.5$    | $0.6 \pm 0.3$    |
| $\alpha x_{rms}$ (mrad) |               |                   | $0.7 \pm 0.2$    |
| $\alpha x_{max}$ (mrad) |               |                   | $1.5 \pm 0.5$    |
| $\alpha y_{rms}$ (mrad) |               |                   | $0.4 \pm 0.1$    |
| $\alpha y_{max}$ (mrad) |               |                   | $0.8 \pm 0.3$    |
| $\eta x @inj.$ (cm)     | 0             | $3.3 \pm 2.6$     | $-0.1 \pm 0.2$   |
| $\eta y @inj.$ (cm)     | 0             | $7.9 \pm 12.4$    | $-0.4 \pm 0.4$   |

**TABLE VII**  
**Closed orbit parameters before and after correction**  
**10 monitors, 8 correctors (sextupoles on)**

$$\Delta x = \Delta y = 0.2 \text{ mm}, \Delta\Theta = \Delta\Phi = 0,25 \text{ mrad}, \Delta B/B = 5 \times 10^{-4}$$

|                         | ideal machine | before correction | after correction |
|-------------------------|---------------|-------------------|------------------|
| $X_{rms}$ (mm)          | 0             | 5.3±3.3           | 0.5±0.2          |
| $X_{max}$ (mm)          | 0             | 9.0±4.9           | 1.4±0.3          |
| $Y_{rms}$ (mm)          | 0             | 3.0±1.4           | 0.2±0.1          |
| $Y_{max}$ (mm)          | 0             | 5.5±2.3           | 0.5±0.2          |
| $\eta x_{rms}$ (cm)     | 66.4          | 65.6±0.2          | 65.5±0.1         |
| $\eta x_{max}$ (cm)     | 100.3         | 104.8±1.9         | 102.2±0.9        |
| $\eta y_{rms}$ (cm)     | 0             | 5.2±2.7           | 1.7±0.9          |
| $\eta y_{max}$ (cm)     | 0             | 8.9±4.3           | 3.2±1.7          |
| $\alpha x_{rms}$ (mrad) |               |                   | 0.7±0.2          |
| $\alpha x_{max}$ (mrad) |               |                   | 1.5±0.6          |
| $\alpha y_{rms}$ (mrad) |               |                   | 0.4±0.1          |
| $\alpha y_{max}$ (mrad) |               |                   | 0.8±0.3          |
| $Q_x$                   | 2.89          | 2.887±.008        | 2.890±.002       |
| $Q_y$                   | 1.13          | 1.131±.002        | 1.131±.002       |
| $\eta x @inj.$ (cm)     | 0             | -2.4±2.3          | -0.1±0.6         |
| $\eta y @inj.$ (cm)     | 0             | -3.5±7.4          | 1.1±2.4          |

**TABLE VIII**  
**Closed orbit parameters before and after correction**  
**10 monitors, 8 correctors (sextupoles on)**

$$\Delta x = \Delta y = 0.2 \text{ mm}, \Delta\Theta = \Delta\Phi = 0,25 \text{ mrad}, \Delta B/B = 5 \times 10^{-4}$$

**Monitor alignment errors  $\Delta x = \Delta y = 0.2 \text{ mm}$**

|                         | ideal machine | before correction | after correction |
|-------------------------|---------------|-------------------|------------------|
| $X_{rms}$ (mm)          | 0             | 5.3±3.3           | 0.6±0.2          |
| $X_{max}$ (mm)          | 0             | 9.0±4.9           | 1.4±0.5          |
| $Y_{rms}$ (mm)          | 0             | 3.0±1.4           | 0.2±0.1          |
| $Y_{max}$ (mm)          | 0             | 5.5±2.3           | 0.6±0.2          |
| $\eta x_{rms}$ (cm)     | 66.4          | 65.6±0.2          | 65.5±0.1         |
| $\eta x_{max}$ (cm)     | 100.3         | 104.8±1.9         | 102.6±0.8        |
| $\eta y_{rms}$ (cm)     | 0             | 5.2±2.7           | 1.8±1.0          |
| $\eta y_{max}$ (cm)     | 0             | 8.9±4.3           | 3.4±1.8          |
| $\alpha x_{rms}$ (mrad) |               |                   | 0.8±0.2          |
| $\alpha x_{max}$ (mrad) |               |                   | 1.5±0.6          |
| $\alpha y_{rms}$ (mrad) |               |                   | 0.4±0.1          |
| $\alpha y_{max}$ (mrad) |               |                   | 0.8±0.3          |
| $Q_x$                   | 2.89          | 2.887±.008        | 2.891±.002       |
| $Q_y$                   | 1.13          | 1.131±.002        | 1.131±.002       |
| $\eta x @inj.$ (cm)     | 0             | -2.4±2.3          | -0.1±0.6         |
| $\eta y @inj.$ (cm)     | 0             | -3.5±7.4          | 1.1±2.6          |

From the results of the above described simulations we can conclude that the "first day" injection can be performed without orbit correction with or without chromaticity correction. Quadrupoles will be provided with mechanical adjustments in both transverse planes, so that a "first order" correction will strongly reduce the closed orbit. The magnetic correctors (even designed to correct the full orbit foreseen with the assumed alignment tolerances,  $\alpha_{\max} \approx 2$  mrad) will then help in maintaining the orbit within the desired limits, or to perform beam displacement for diagnostic and injection optimization during commissioning.

## 5 - FIELD INDEX ERRORS

Particular attention has been paid to the sensitivity of the lattice to field index errors in the bending magnet. A nominal value of  $n=0.5$ , corresponding to a gradient of 0.7 T/m is beneficial to the behaviour of the optical functions because of its focusing effect in both planes and gives also the same betatron damping in horizontal and vertical. The obvious drawback of this choice is the increased complexity in the bending magnet design and construction.

In order to estimate the effect of random errors in the pole shape, we have randomly extracted the field index in the eight bending magnets of the accumulator from a uniform distribution within  $\pm 10\%$  with respect to the ideal value. This exercise has been repeated five times, and the optical functions have been calculated with MAD, giving always comparable results. Fig. 12 shows the optical functions of one of the simulated machines with field index errors. The calculated value for the horizontal betatron wavenumber was 2.880 instead of 2.890, while the vertical changed from 1.130 to 1.144. The variation of the optical functions from the ideal ones can be clearly seen, but the variation of the dispersion at the injection septum is limited to a few centimeters, so that injection efficiency should not be affected. In the framework of three independent quadrupole families, we tried then to correct the tunes and the dispersion in the center of one injection region. The resultant optical functions are shown in Fig. 13, from which it can be seen that the perturbation on the optical functions is worse than in the previous case, although the maximum  $\beta$  values in both planes do not change by more than 20% with respect to the nominal ones. We tried also a more sophisticated correction with 6 independent quadrupole families (2 focusing and 4 defocusing) to cancel the variation of the tunes, of the dispersion and of its derivative in both injection straights. The result presented in Fig. 14 shows a larger increase in the vertical  $\beta$  function, which almost reaches 20 m.

From magnetic measurements it is obviously possible to choose the best sequence in the lattice to avoid excessive variations of the optical functions. We have tried all the possible combinations on one of the field index error distributions. The best result is shown in Fig. 15: the variation of the  $\beta$  functions is still observable, but their maximum values are almost the same as the ideal ones.

To establish the maximum tolerance on the field index error, the above described simulations have been repeated with a  $\pm 20\%$  error distribution. The optical functions after correction of the tunes and dispersion in one of the two injection straights are plotted in Fig. 16, showing a much larger distortion, particularly in the case of the dispersion derivative in the injection straights.

Our conclusion is that a  $\pm 10\%$  error in the field index can be handled for the accumulator. A larger error would require complicated correction procedures.

## 6 - HIGH ORDER MULTIPOLES IN THE MAGNETIC FIELDS

A first attempt has been made to establish the order of magnitude of the tolerance on magnetic field quality by looking at the dynamic aperture dependence on multipole intensity. Two sextupole families have been used to correct the chromaticity in order to avoid the head-tail instability and to improve the energy acceptance of the accumulator. The sextupole positions in the lattice are shown in Figs. 1-2. Fig. 17 shows the dynamic aperture for the ideal machine with sextupoles, calculated in the center of the injection straight section with the code PATRICIA, for particles with the nominal energy, with  $\Delta E/E = +1.5\%$  and with  $\Delta E/E = -1.5\%$ : the shaded area corresponds to stable oscillation for all the particles within the required energy range. The available aperture, taking into account that the horizontal  $\beta$  at the straight section center is  $\approx 1/4$  of its maximum value, is larger than the vacuum chamber physical limit.

To give an estimate of the tolerable multipoles in bending magnets and quadrupoles, we looked for the stable amplitudes in the horizontal and vertical planes separately as a function of the intensity of the most dangerous multipole components. Each multipole has been considered as the only source of field error, and the effect on particles with the nominal energy and with the maximum energy deviations ( $\pm 1.5\%$ ) has been simulated. In all the following figures the maximum stable oscillation amplitude is plotted as a function of the relative field variation  $\Delta B/B$  at a distance of 3 cm from the center of the magnet. In the bending magnet sextupole, octupole (due to the field index and the small bending radius) and decapole have been studied. Their effect is shown in Figs. 18-20. The sextupole component does not seem to be dangerous (and of course can be corrected with the pure sextupoles used for chromaticity correction), while octupole and decapole tend to strongly affect the dynamic aperture. Assuming as tolerable a reduction of 20% in the horizontal plane (the vertical stable region exceeds by a large factor the physical aperture), both octupole and decapole components should not exceed  $\Delta B/B = 10^{-4}$  at 3 cm from the center. The situation is less demanding for the quadrupoles, where octupole and 12-pole effects have been studied. The behaviour of stable oscillations is shown in Figs. 21-22. Assuming the same criterion of the bending magnet, a tolerance of  $5 \times 10^{-4}$  at 3 cm from the center is still acceptable.

It is clear that setting the tolerances in this way is safe, but probably it will be possible to relax somewhat these limits, because different multipoles can combine in such a way to affect the dynamic aperture less than their worst combination. The only way to proceed is to design the bending magnet trying to have multipoles near the indicated limits, and then check by tracking the dynamic aperture.

## REFERENCES

- [1] M. Preger: "A positron and electron accumulator for DAΦNE" - DAΦNE Technical Note I-1 (8/11/90).
- [2] M. Biagini: "DAΦNE accumulator ring dynamic aperture" - DAΦNE Technical Note L-2 (4/4/91).

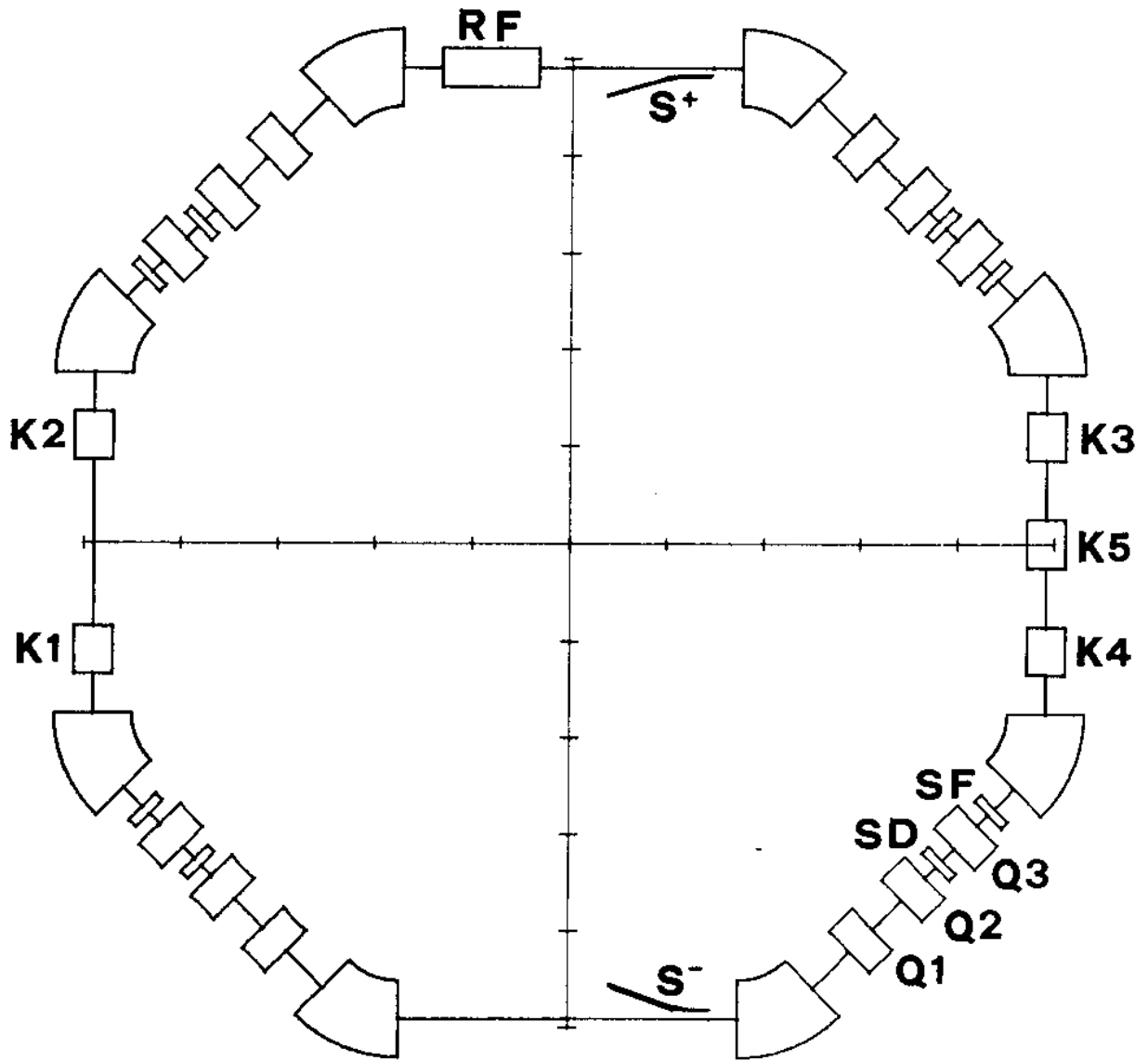


Fig. 1 - Schematic layout of the accumulator ring.

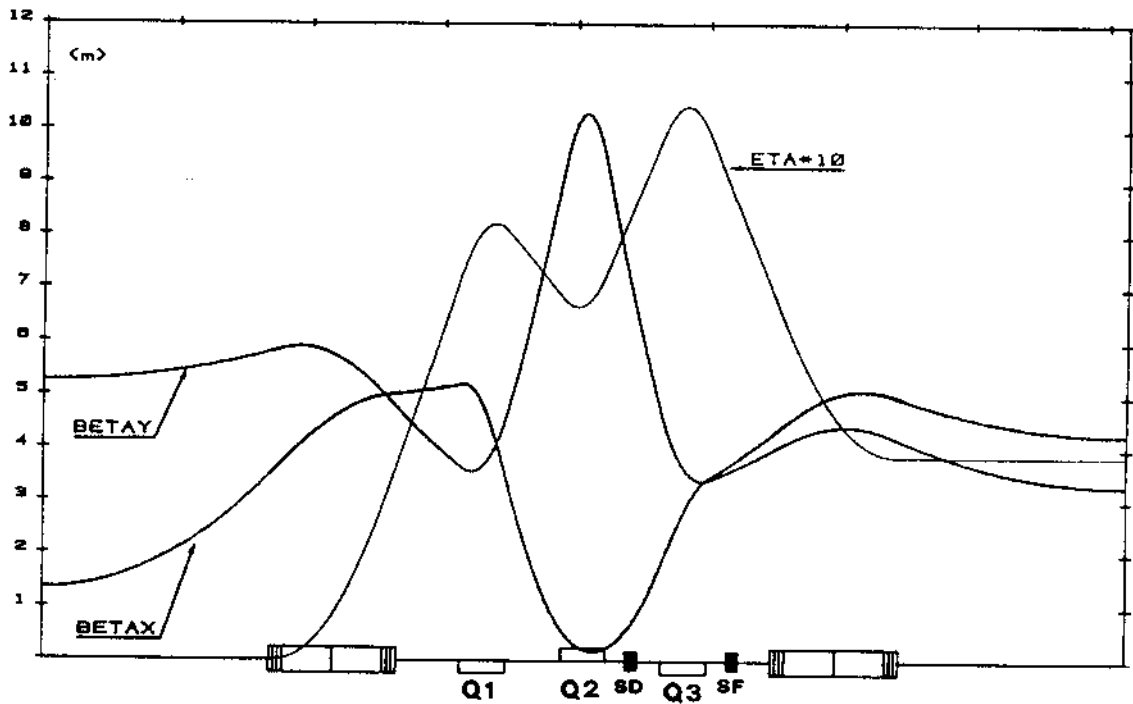


Fig. 2- Optical functions for 1/4 of the ring. Injection straight section on the left.

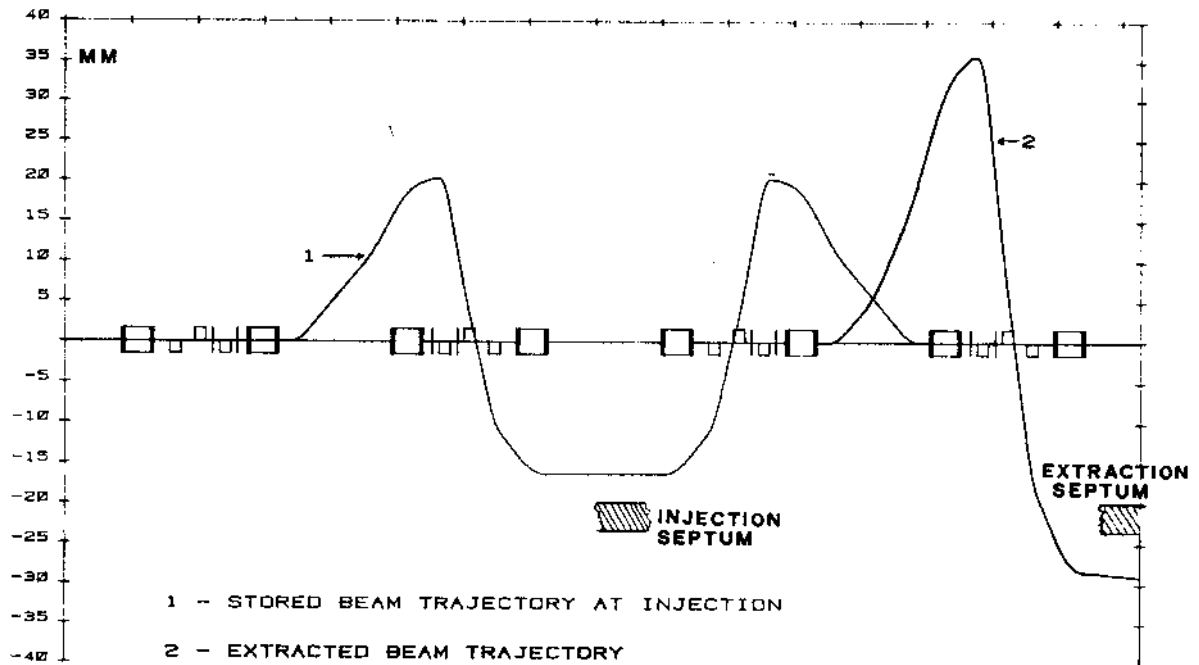


Fig. 3 - Kicker induced trajectories of the stored beam at injection and extraction.

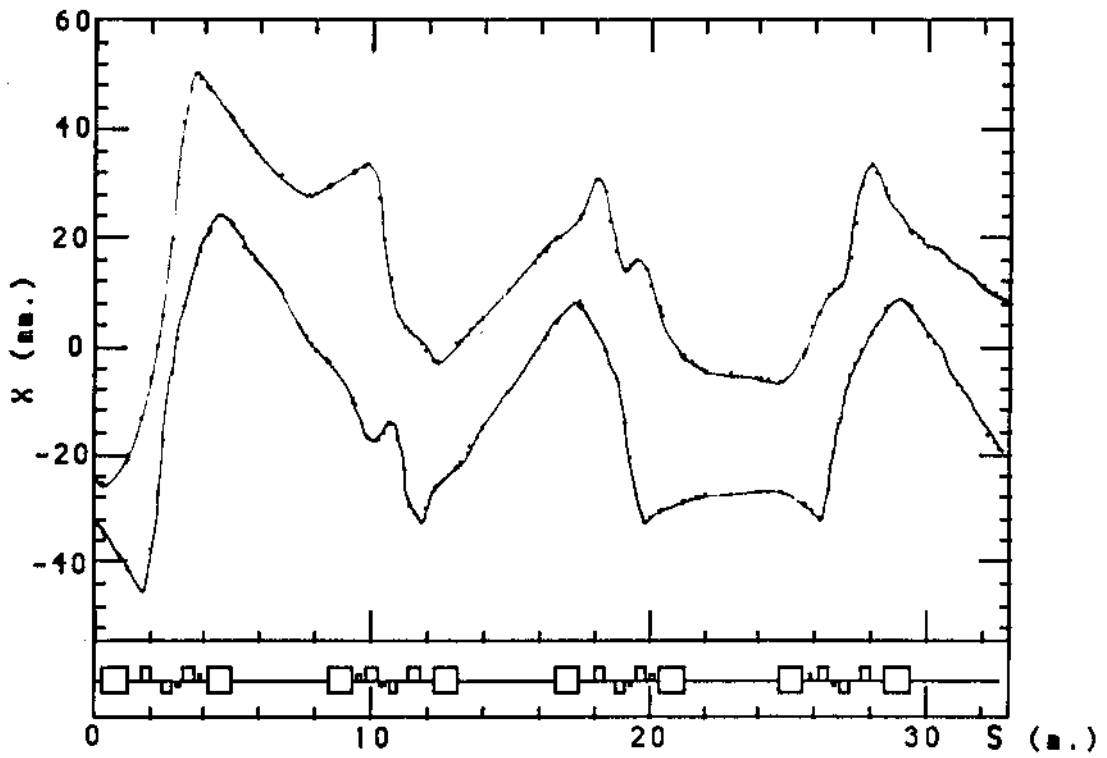


Fig. 4 - Horizontal envelope for 1000 particles at the first turn.

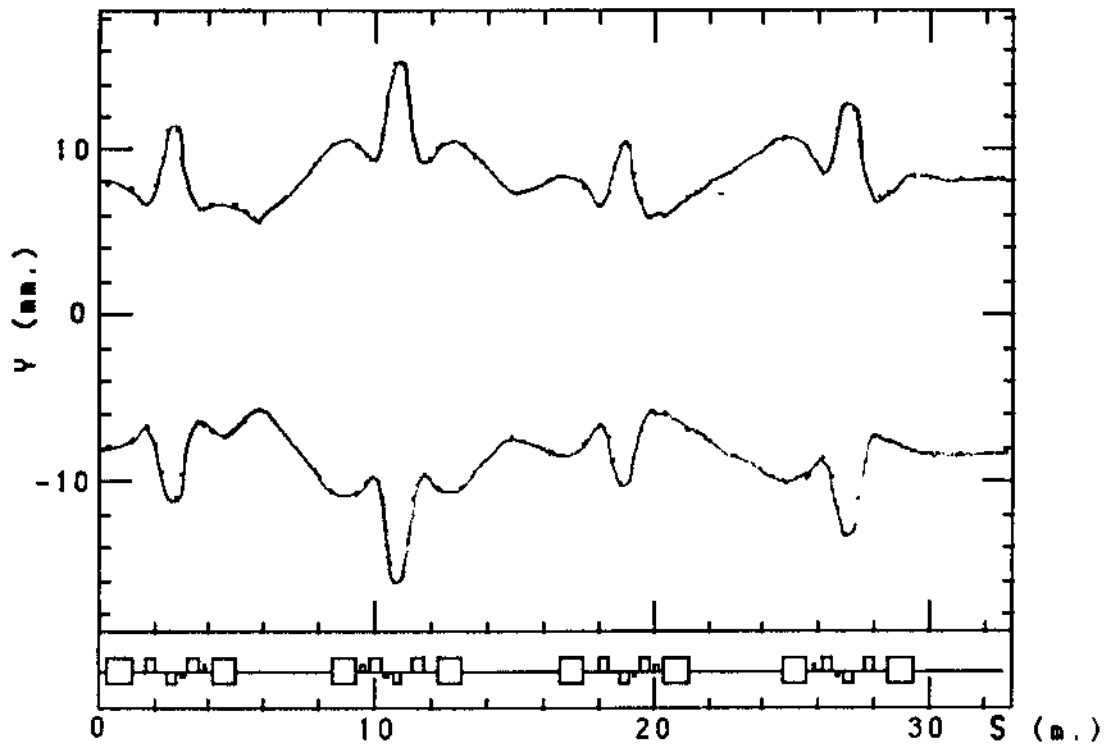


Fig. 5 - Vertical envelope for 1000 particles at the first turn.

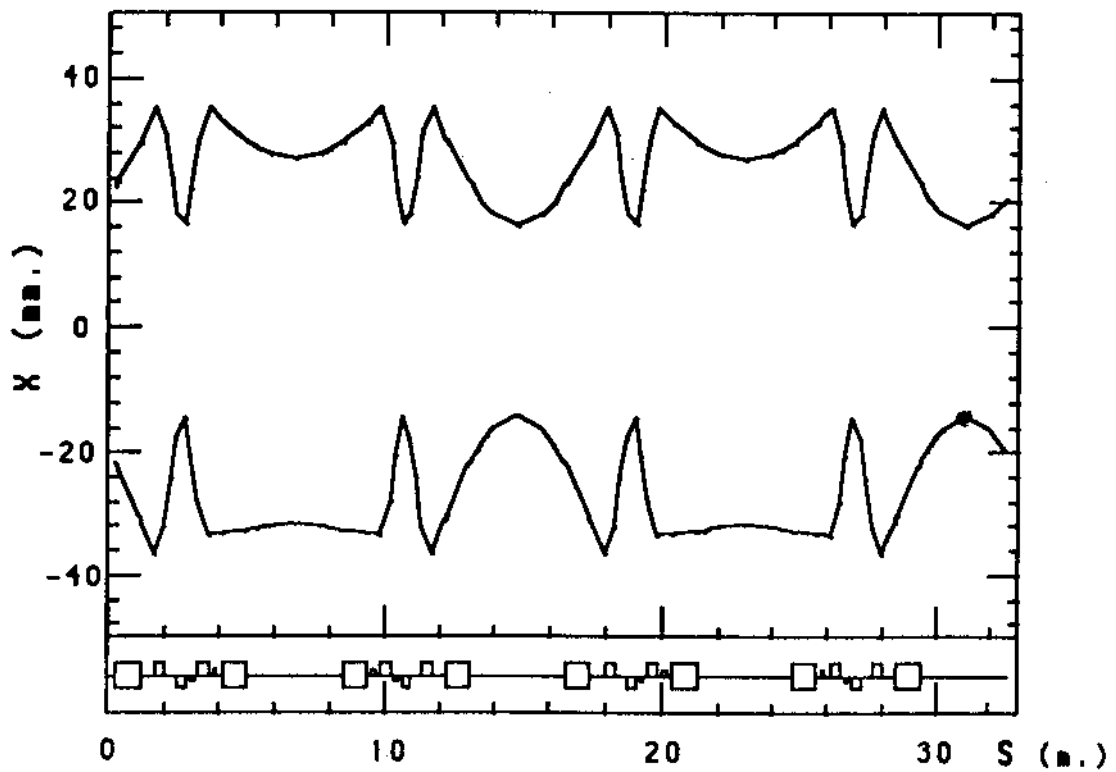


Fig. 6 - Maximum horizontal envelope for 1000 particles tracked through 500 turns (excluding the first one). The number of particles escaping the injection septa is 998.

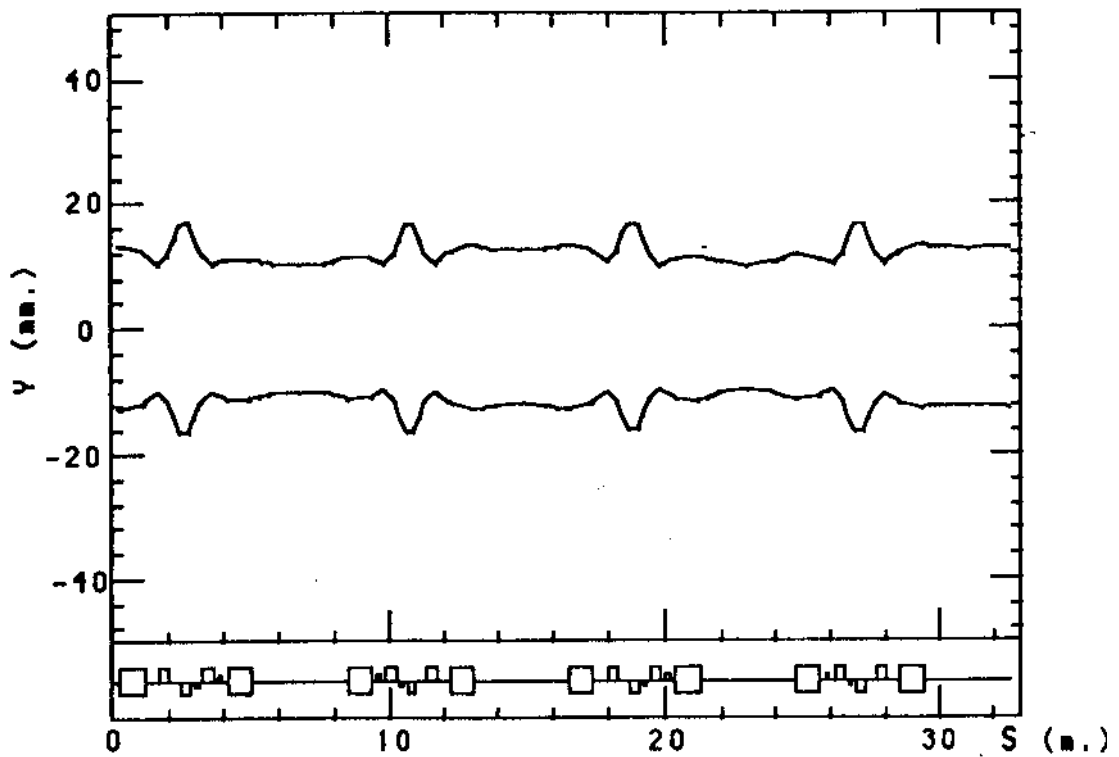


Fig. 7 - Maximum vertical envelope for 1000 particles tracked through 500 turns (excluding the first one). The number of particles escaping the injection septa is 998.

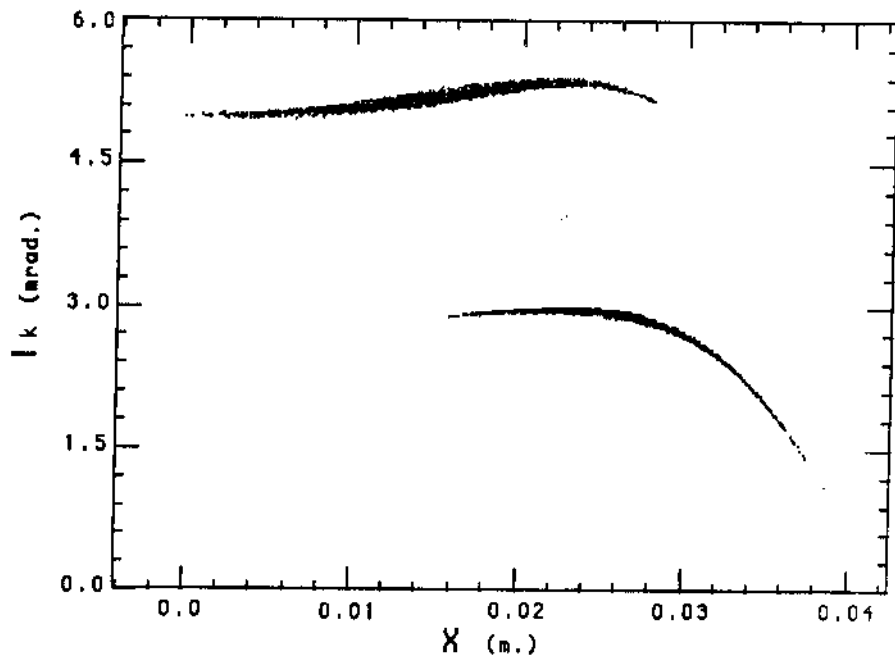


Fig. 8 - Angular deflection at the kickers as a function of the horizontal particle position.

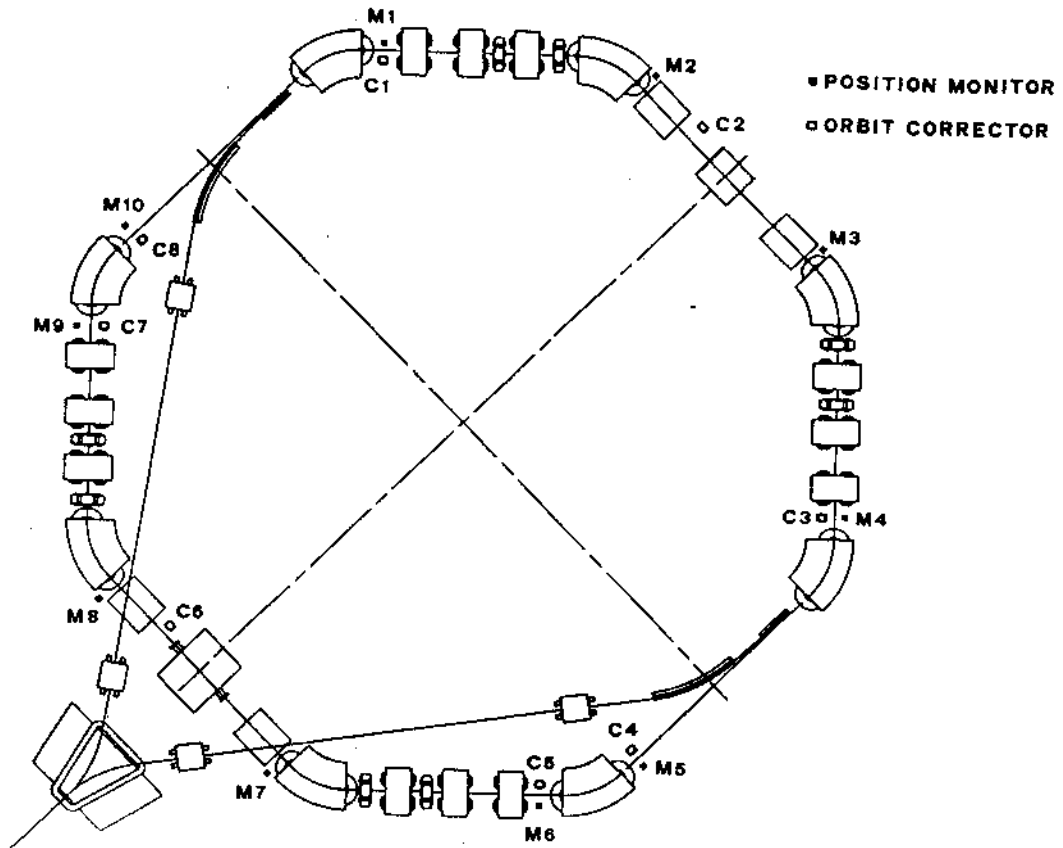


Fig. 8 /A - Beam position monitor and orbit corrector layout.

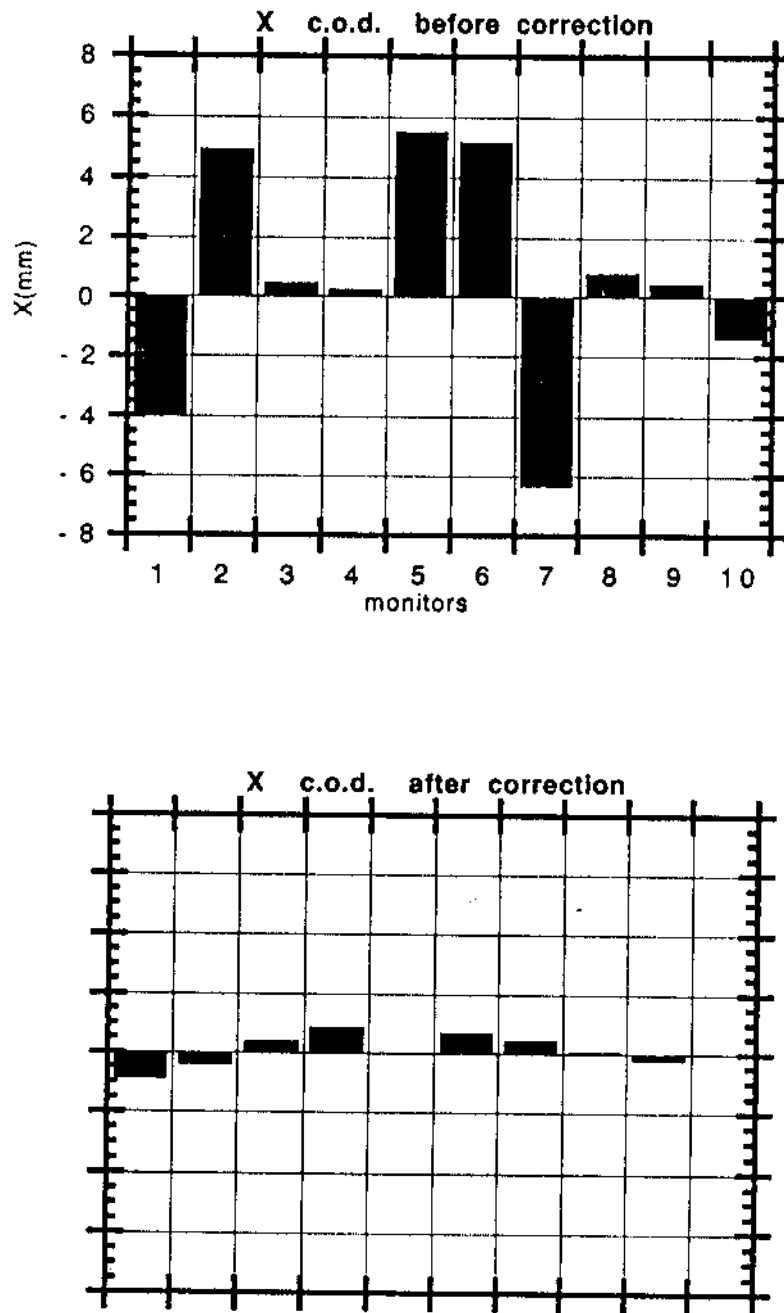
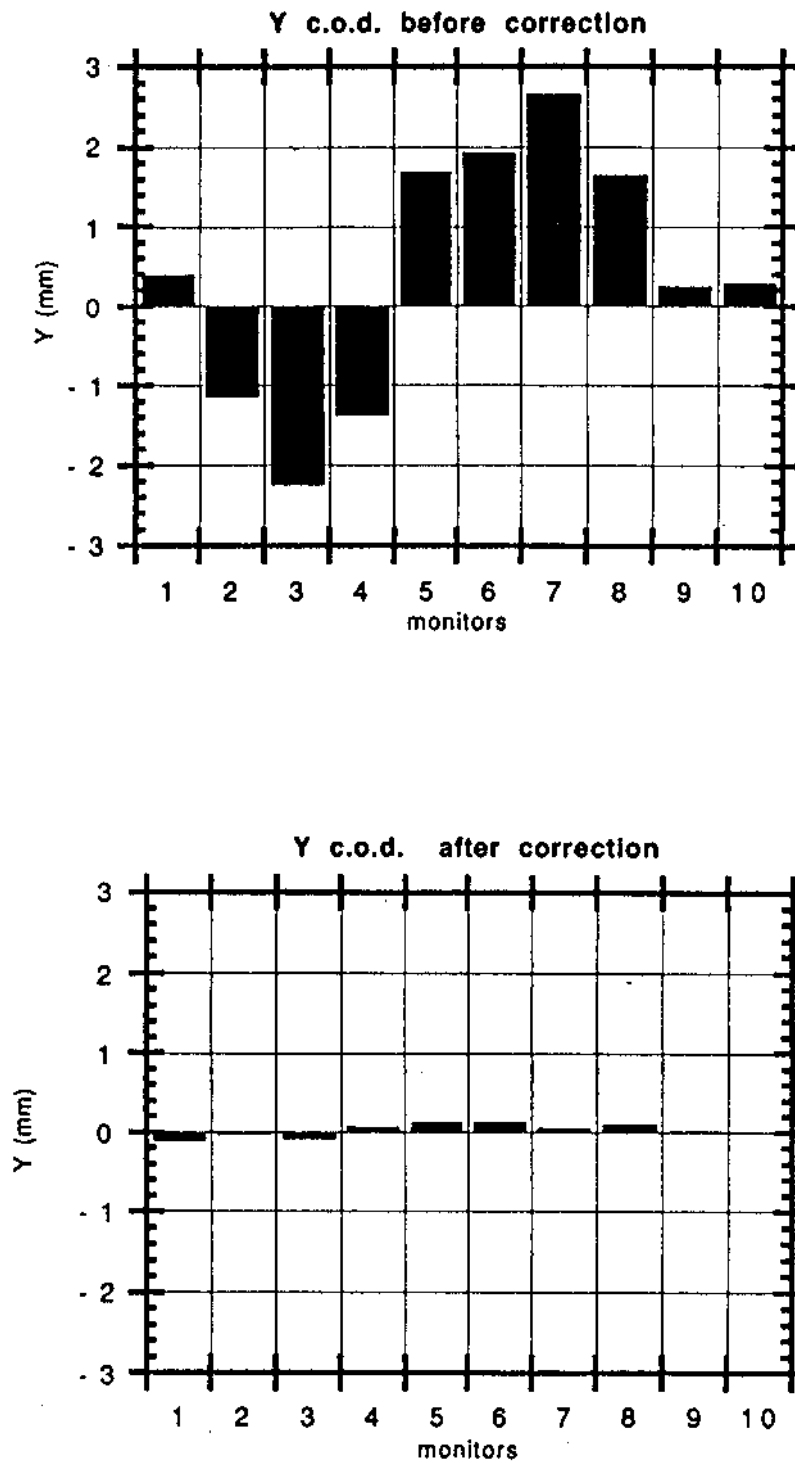


Fig. 9 - Beam position at the monitors before and after orbit correction in the horizontal plane.



*Fig. 10- Beam position at the monitors before and after orbit correction in the vertical plane.*

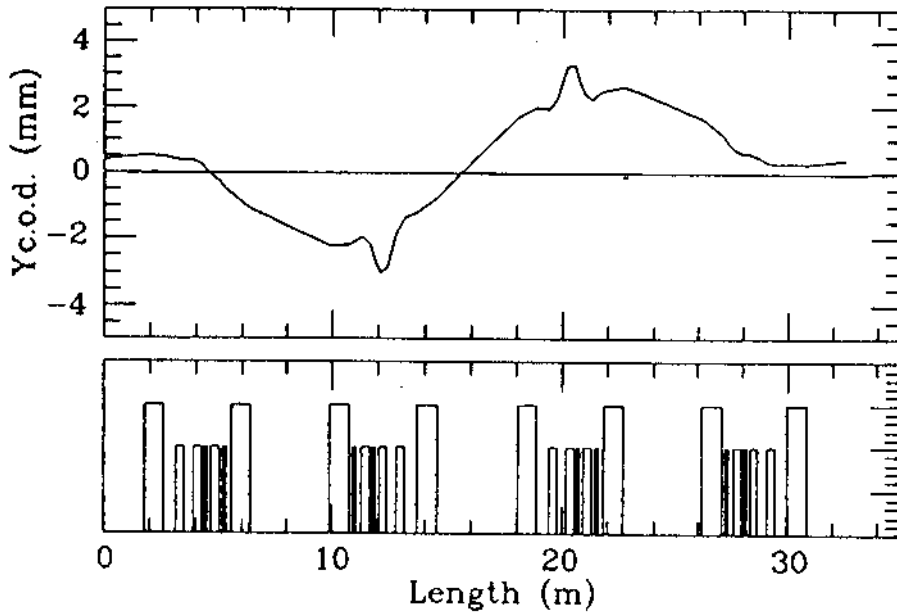
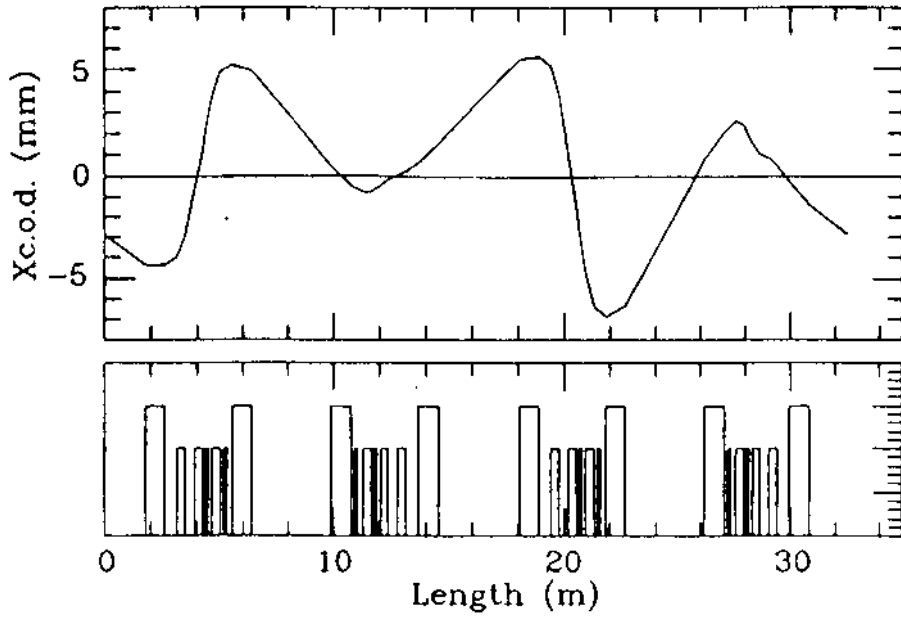


Fig. 11 - Uncorrected closed orbit predicted by MAD.

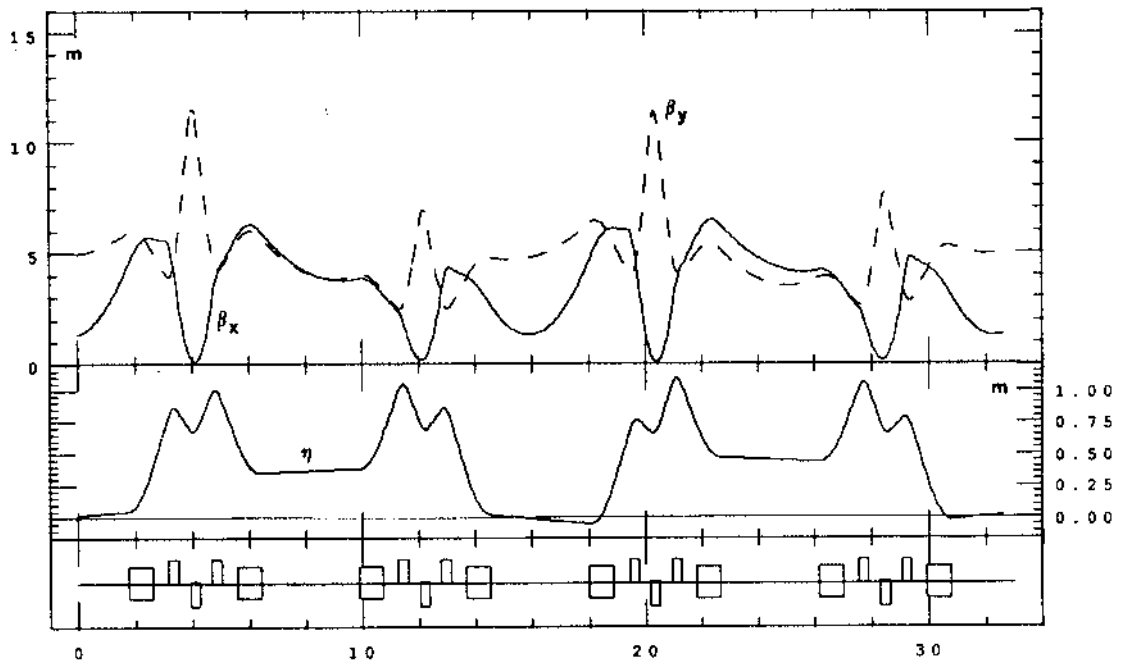


Fig. 12 - Optical functions with  $\pm 10\%$  field index errors.

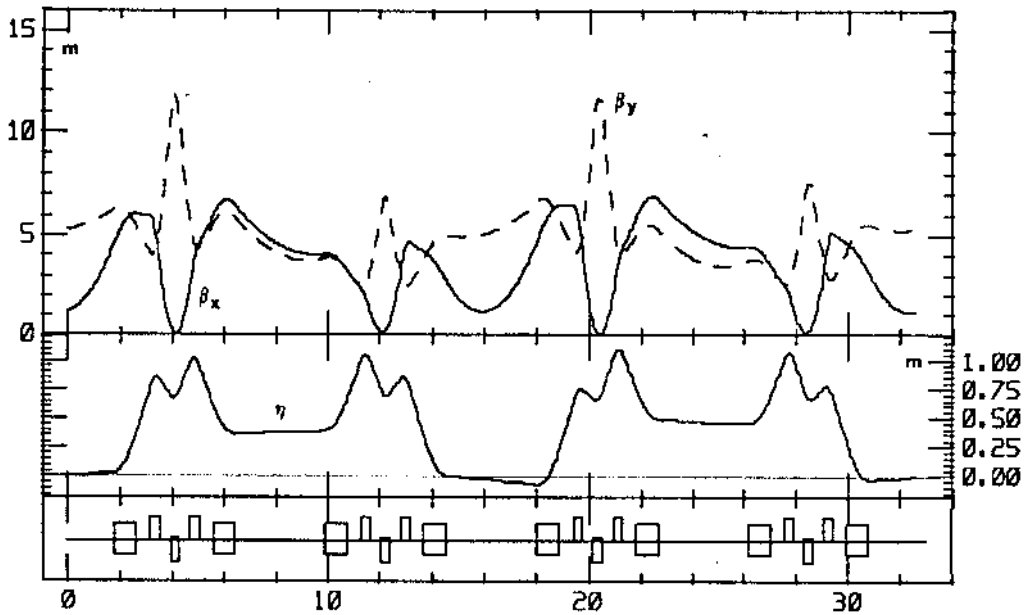


Fig. 13 - Optical functions with  $\pm 10\%$  field index errors and correction of the tunes and dispersion in one injection section with 3 quadrupole families.

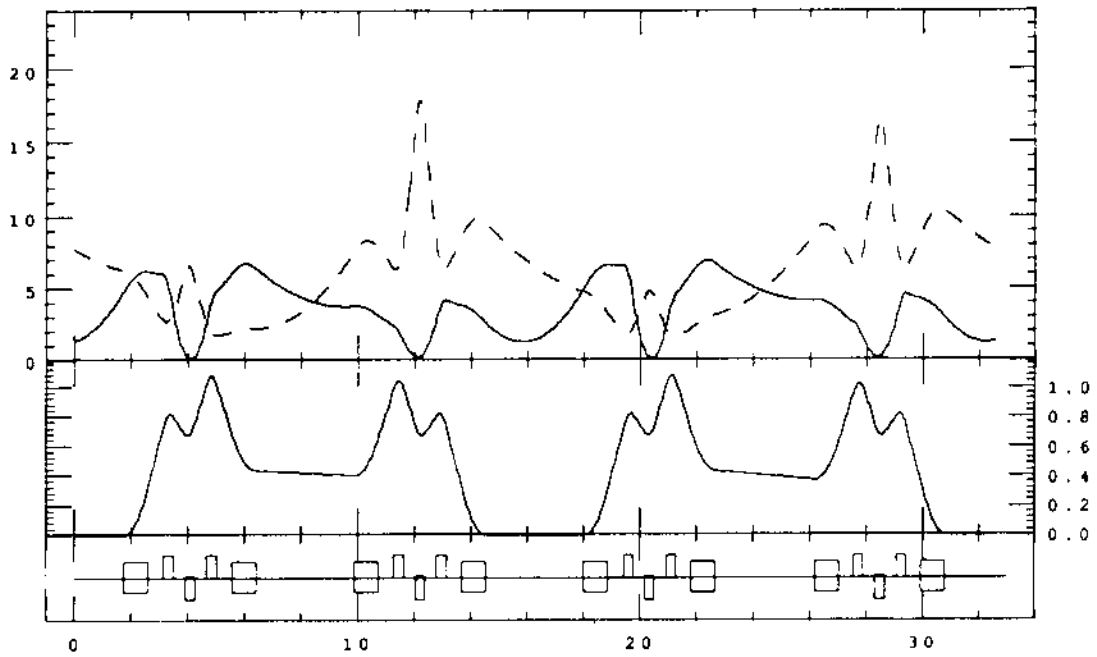


Fig. 14 - Optical functions with  $\pm 10\%$  field index errors and correction of the tunes, dispersion and its derivative in both injection straight sections with 6 quadrupole families.

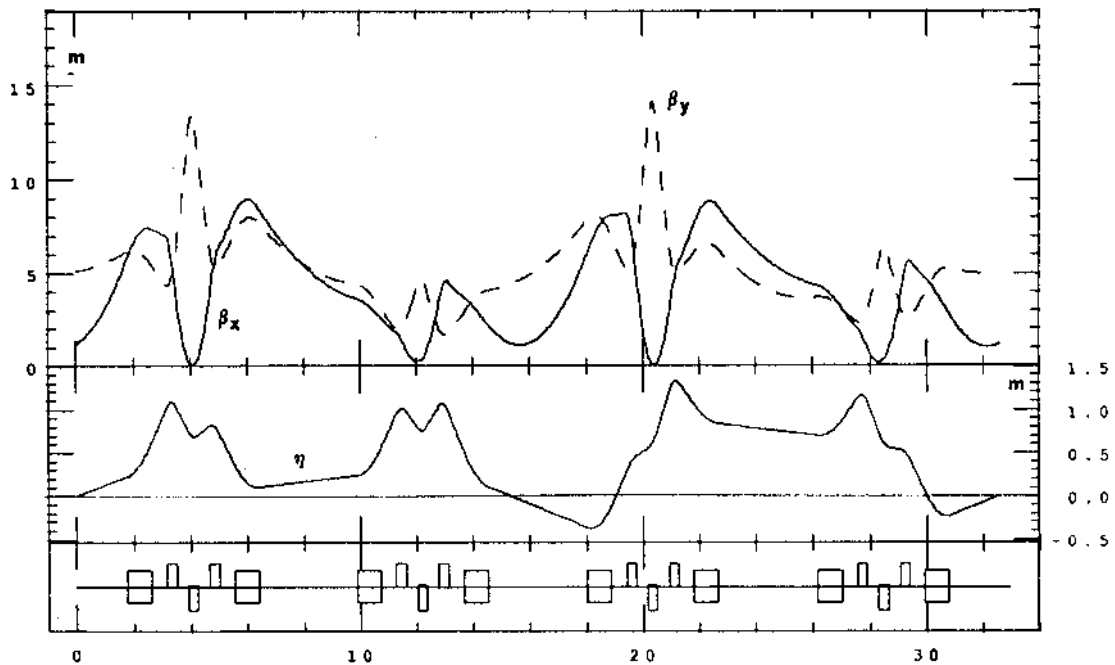


Fig. 15 - Optical functions with  $\pm 10\%$  field index errors and correction of the tunes, dispersion and its derivative in both injection straight sections with 6 quadrupole families, and best choice of magnet arrangement.

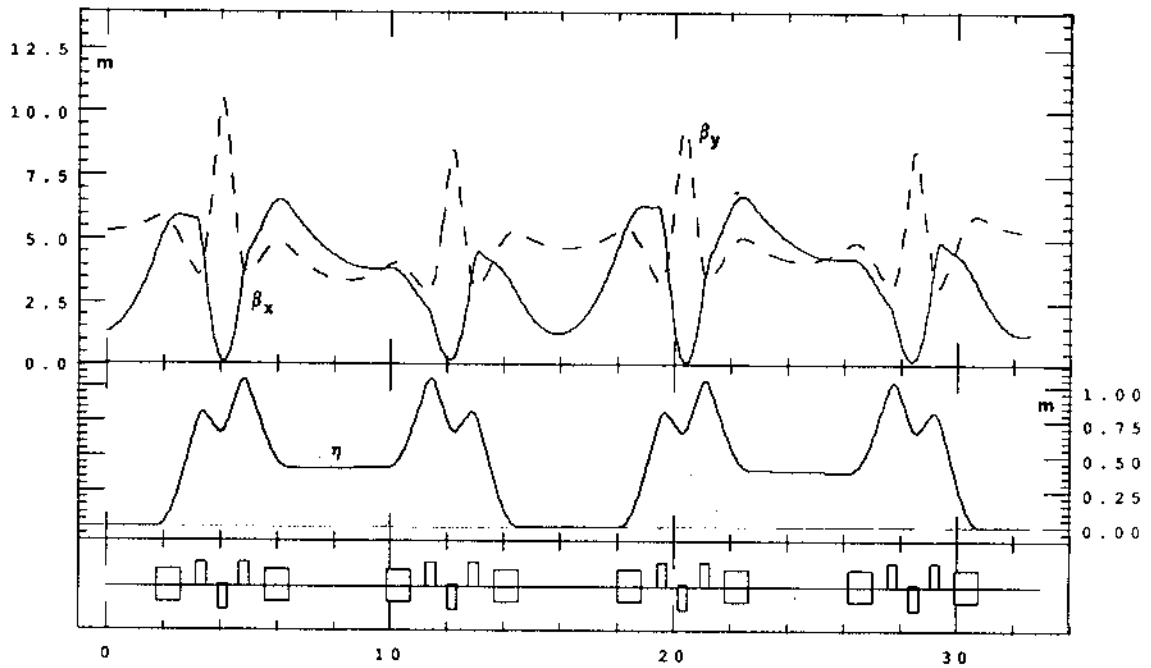


Fig. 16 - Optical functions with  $\pm 20\%$  field index errors and correction of the tunes and dispersion in one injection straight section with 3 quadrupole families.

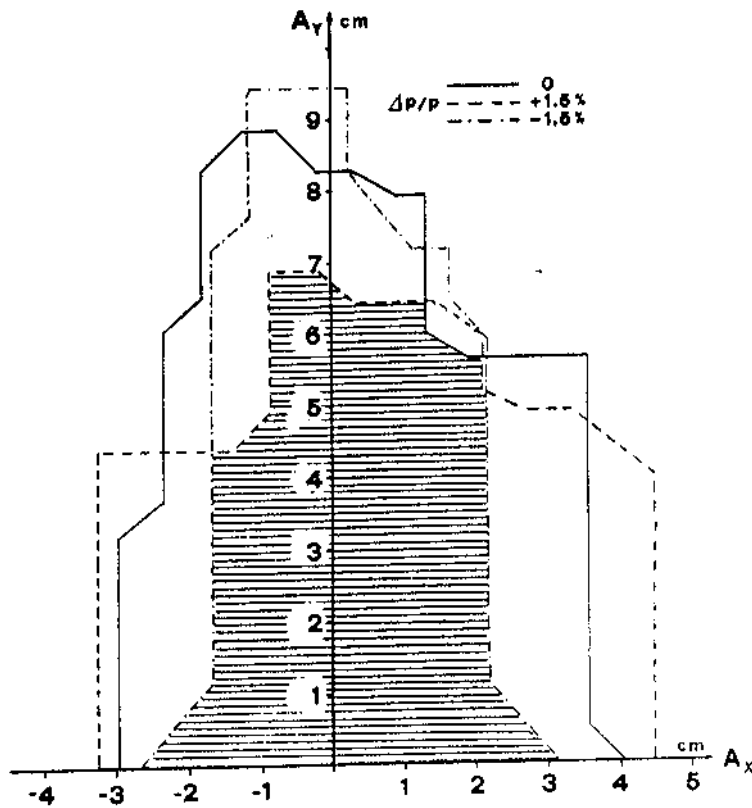
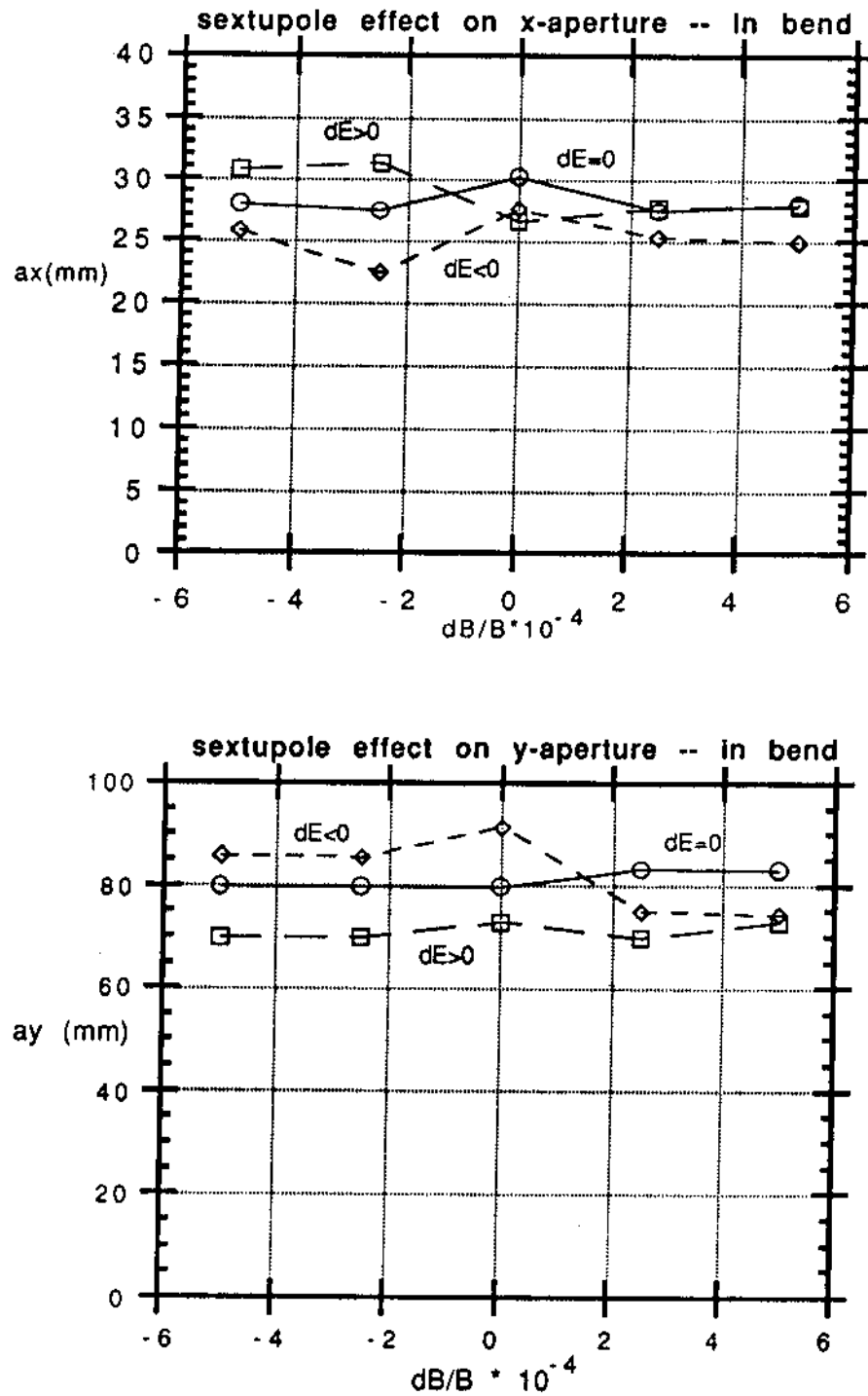


Fig. 17 - Dynamic aperture for the ideal machine, calculated in the center of the injection straight section. The chromaticity in both planes is  $+1.0$ . The shaded area is the stable space within  $\pm 1.5\%$  energy deviation.



*Fig. 18 - Dynamic apertures in the horizontal and vertical planes as a function of sextupole component in the bending magnet field. Errors are taken at 3 cm from the magnet center.*

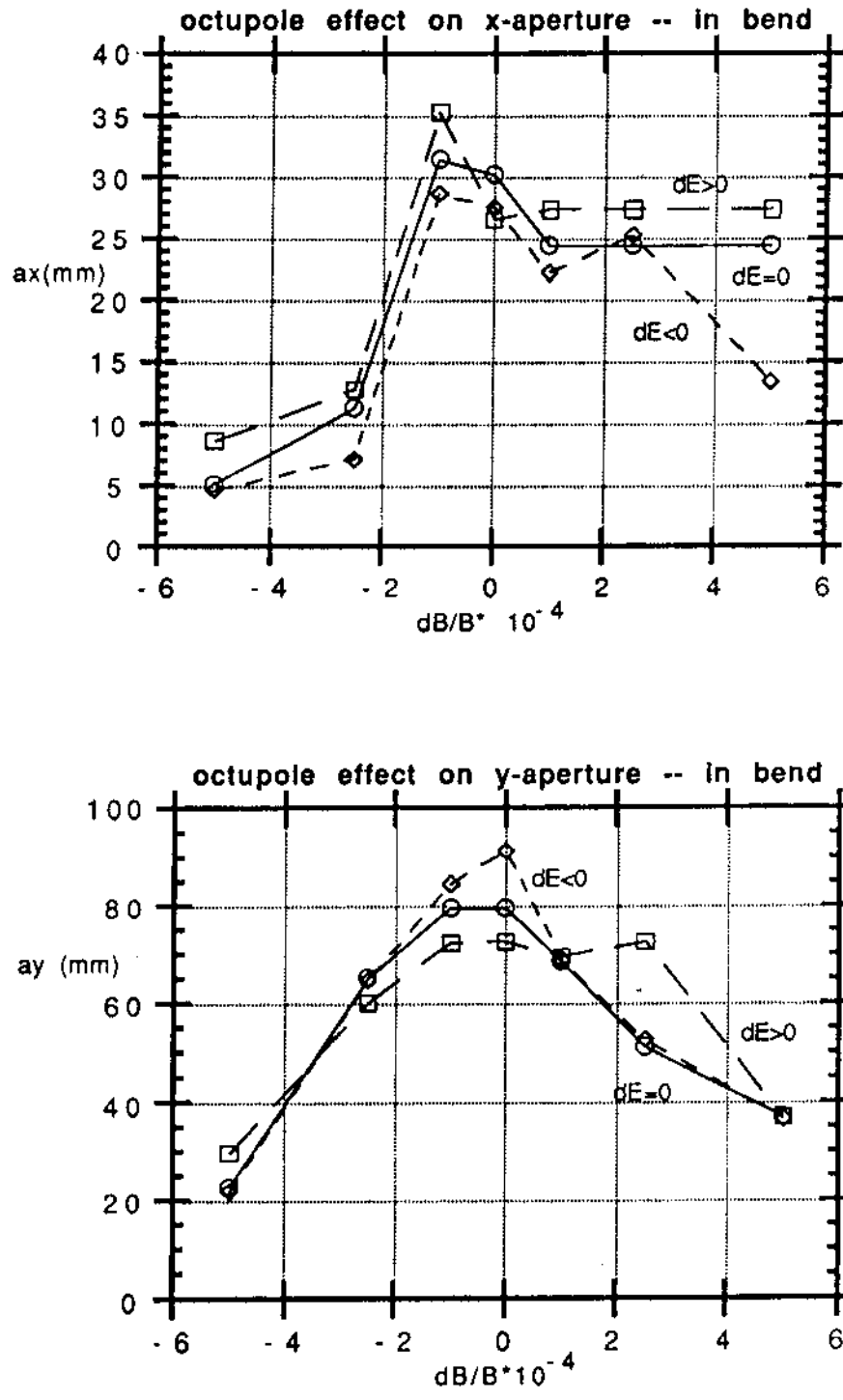


Fig. 19 - Dynamic apertures in the horizontal and vertical planes as a function of octupole component in the bending magnet field. Errors are taken at 3 cm from the magnet center.

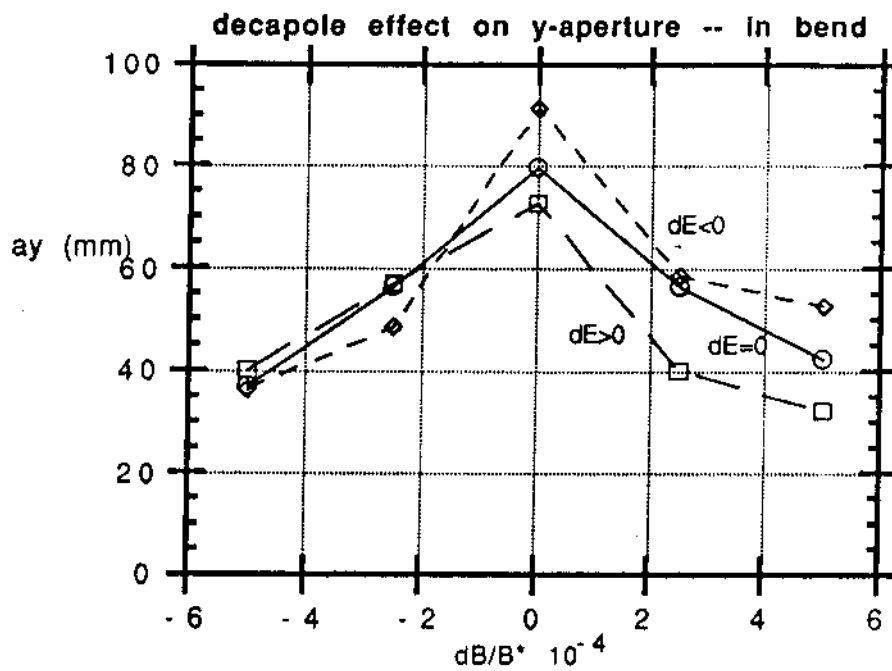
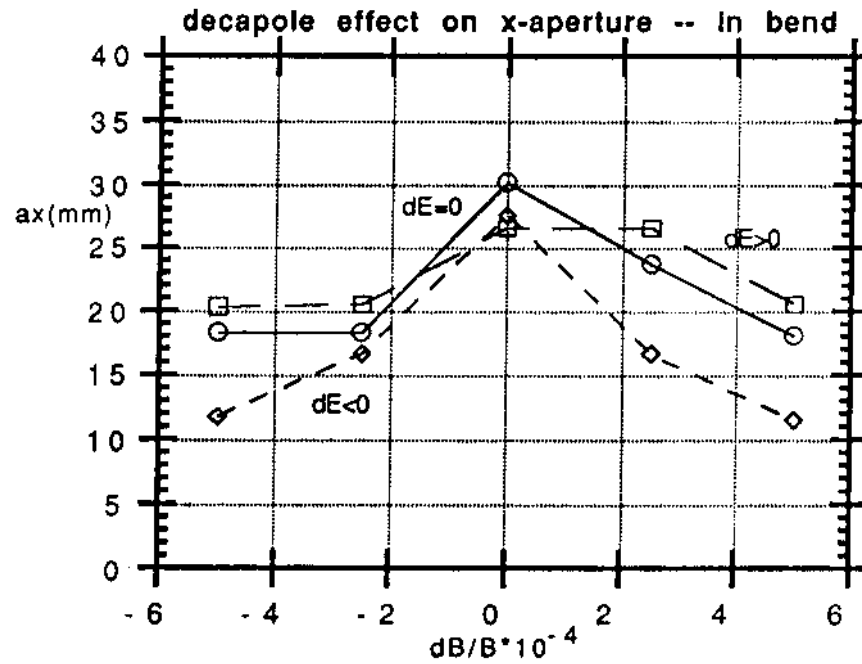


Fig. 20 - Dynamic apertures in the horizontal and vertical planes as a function of decapole component in the bending magnet field. Errors are taken at 3 cm from the magnet center.

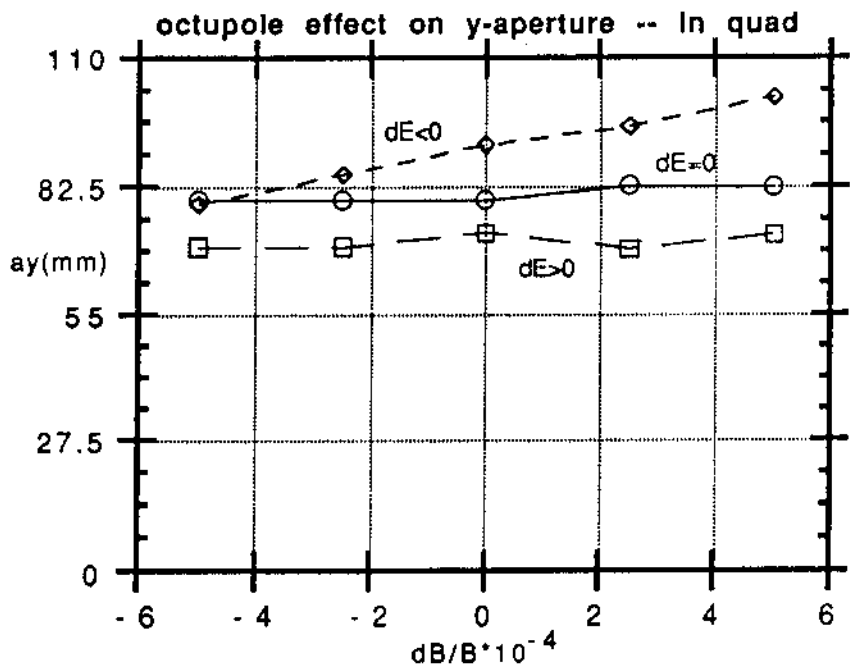
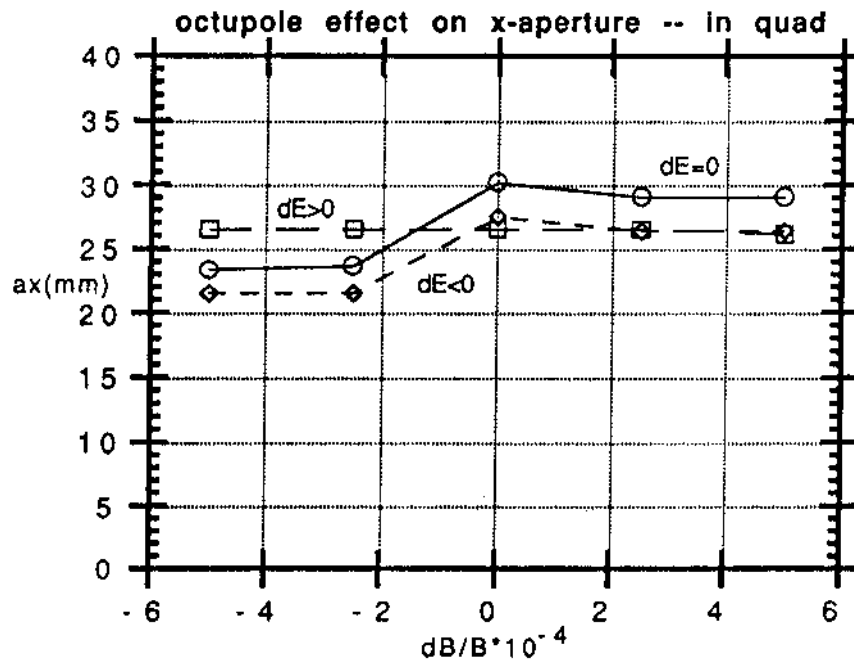
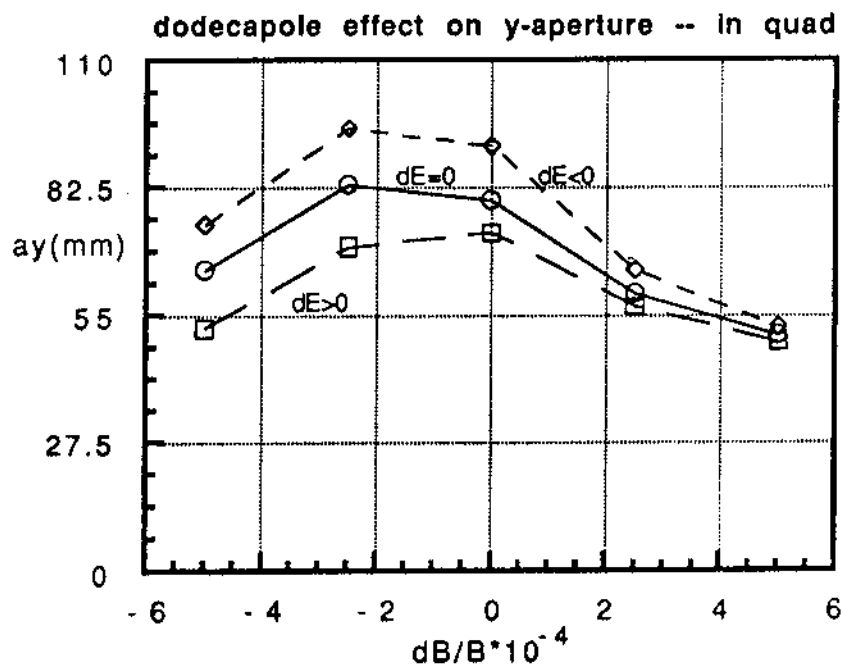
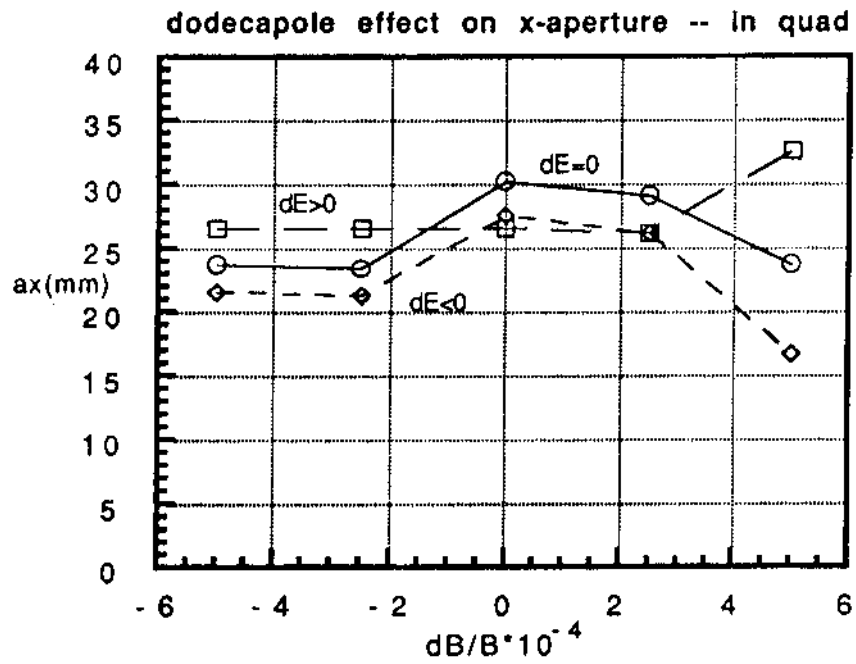


Fig. 21 - Dynamic apertures in the horizontal and vertical planes as a function of octupole component in the quadrupole field. Errors are taken at 3 cm from the magnet center.



*Fig. 22 - Dynamic apertures in the horizontal and vertical planes as a function of 12-pole component in the quadrupole field. Errors are taken at 3 cm from the magnet center.*